Pergamon

Int. J. Heat Mass Transfer. Vol. 40, No. 15, pp. 3689–3701, 1997

Printed in Great Britain
0017–9310/97 $17.00+0.00

PII: S0017–9310(97)00004–5

Laminar convective heat transfer of a Bingham plastic in a circular pipe—II. Numerical approach—hydrodynamically developing flow and simultaneously developing flow

TAEGEE MIN, HYOUNG GWON CHOI, JUNG YUL YOO† and HAECHEON CHOI

Department of Mechanical Engineering, Seoul National University, Seoul 151-742, Korea

(*Received* 19 *April* 1996 *and in final form* 18 *October* 1996)

Abstract—Hydrodynamically developing and simultaneously (that is, hydrodynamically and thermally) developing laminar flows of a Bingham plastic in a circular pipe have been investigated numerically. Solutions have been obtained by using a four-step fractional method combined with an equal order bilinear finite element method. For hydrodynamically developing flow, shorter entrance length is required to reach fully developed velocity field and thicker unyielded region appears closer to the inlet as the yield stress becomes larger. For simultaneously developing flow, the heat transfer characteristics show the same trends as those predicted from the thermally developing flow. © 1997 Elsevier Science Ltd.

1. INTRODUCTION

There are four types of laminar duct flows, namely, fully developed, hydrodynamically developing, thermally developing and simultaneously (that is, hydrodynamically and thermally) developing flows [1–3]. In Part I of the present work [4], we studied thermally fully developed flow and thermally developing flow (the Graetz problem extended) of a Bingham plastic in a circular pipe using analytical methods. The classical Graetz problem generally provides fundamental references for thermal devices. However, in most industrial applications more complex fully elliptic governing equations are involved than those of the idealized Graetz problem.

Chen *et al.* [5] studied hydrodynamically developing flow of a Bingham plastic in a circular pipe using the boundary layer equations. However, as McDonald *et al.* [6] and Vradis *et al.* [7] pointed out, the boundary layer equations fail to predict the flow characteristics near the inlet, such as the adverse pressure gradients and the velocity overshoots, because these equations neglect the pressure variation in the radial direction of a pipe. Recently, Vradis *et al.* [7] reported numerical solutions for hydrodynamically developing and simultaneously developing flow problems by employing the fully elliptic governing equations for a Bingham plastic in a circular pipe, but some errors are found in their approach, as will be illustrated later in the present study.

The purpose of the present study is to investigate hydrodynamically developing and simultaneously developing flows of a Bingham plastic in a circular pipe by a numerical method, which uses a four-step fractional method combined with an equal order bilinear finite element method [8]. Effects of the yield stress, the Prandtl, Reynolds and Brinkman numbers are presented and compared with previous studies.

2. GOVERNING EQUATION

The governing equations for unsteady, laminar, incompressible flow are:

$$\frac{\partial U_i}{\partial x_i} = 0 \tag{1}$$

$$\rho\frac{\partial U_i}{\partial t} + \rho\frac{\partial}{\partial x_j}U_iU_j = -\frac{\partial P}{\partial x_i} + \frac{\partial \tau_{ij}}{\partial x_j} \tag{2}$$

$$\rho C_p\frac{\partial T}{\partial t} + \rho C_p\frac{\partial}{\partial x_j}TU_j = k\frac{\partial^2 T}{\partial x_j^2} + \eta\cdot\Phi \tag{3}$$

where Φ is the dissipation function

$$\Phi = \left(\frac{\partial U_i}{\partial x_j} + \frac{\partial U_j}{\partial x_i}\right)\frac{\partial U_i}{\partial x_j}. \tag{4}$$

Introducing the apparent viscosity in the case of a Bingham plastic to describe the non-Newtonian shear property in a manner analogous to the Newtonian viscosity, the tensorial form of the constitutive equation is given by

$$\tau_{ij} = \eta\dot{\gamma}_{ij} \tag{5}$$

† Author to whom correspondence should be addressed.

NOMENCLATURE

A_e	area of an element
Br	Brinkman number, $\mu_0 U_{av}^2/k(T_e-T_w)$
C_p	specific heat at constant pressure
c	dimensionless radius of the plug flow region, or ratio of the yield shear stress to the wall shear stress, τ_y/τ_w
D	pipe diameter
h	heat transfer coefficient based on bulk temperature
k	thermal conductivity
m	exponential growth parameter
N_t	total number of nodes
Nu	local Nusselt number, hD/k
P	pressure
Pe	Peclet number, $2U_{av}R/\alpha$ or $2\,Re\,Pr$
Pr	Prandtl number, $\mu_0/(\rho\alpha)$
p	dimensionless pressure
R	pipe radius
Re	Reynolds number, $\rho U_{av}R/\mu_0$
r	dimensionless radial coordinate, y/R
S_e	surface of an element
$T(y,z)$	temperature
T_e	entrance temperature
$T_m(z)$	bulk temperature
T_w	wall temperature
t, Δt	time and time increment
$\mathbf{U}$, U_i	axial velocity
U_{av}	average axial velocity
$\hat{U}_i$, U_i^*	intermediate velocities
u	dimensionless axial velocity, U/U_{av}
V	radial velocity
v	dimensionless radial velocity, V/U_{av}
w	weighting function
x	dimensionless axial coordinate, z/R
x^+	dimensionless axial coordinate, $(z/R)/Pe$
Y	yield number, $\tau_y R/\mu_0 U_{av}$
y	radial coordinate
z	axial coordinate.

Greek symbols

α	thermal diffusivity
$\dot{\gamma}$, $\dot{\gamma}_{ij}$	rate of strain, $U_{i,j}+U_{j,i}$
$\dot{\gamma}^*$, $\dot{\gamma}_{ij}^*$	dimensionless rate of strain, $u_{i,j}+u_{j,i}$
η	apparent viscosity for a Bingham model
η_{eff}	dimensionless apparent viscosity, η/μ_0
$\Theta(r,x)$	dimensionless temperature, $(T_w-T)/(T_w-T_e)$
$\Theta_m(x)$	dimensionless bulk temperature, $(T_w-T_m)/(T_w-T_e)$
μ_0	plastic viscosity
ρ	density
τ, τ_{ij}	shear stress
τ_w	wall shear stress
τ_y	yield shear stress
Φ	viscous dissipation function
$\phi(r)$	dimensionless temperature, $(T_w-T)/(T_w-T_m)$
φ	normalized variable.

Superscript

n	time level.

Subscript

e	entrance
w	wall.

where $\dot{\gamma}_{ij} = U_{i,j}+U_{j,i}$ is the rate of strain, η is the apparent viscosity [9–12] such that

$$\eta = \begin{cases} \mu_0 + \dfrac{\tau_y}{\sqrt{\frac{1}{2}(\dot{\gamma}:\dot{\gamma})}} & (|\tau| \geqslant \tau_y) \\ \infty & (|\tau| < \tau_y) \end{cases} \tag{6}$$

τ_y is the yield shear stress and μ_0 is the plastic viscosity.

The drawback of the above viscosity function model is that the viscosity is discontinuous at the yield stress and one must impose a large value in place of the infinity, which may cause a numerical instability in the low shear rate region. Furthermore, this model cannot describe the behavior of a Bingham plastic properly in the low shear region and the unyielded region because it includes only two parameters. Recently, Ellwood *et al.* [13] and Abdali *et al.* [14] who, respectively, studied the laminar jet flow and entry and exit flows of Bingham fluids, reported that this problem can be circumvented by using the following constitutive equation proposed by Papanastasiou [15]

$$\eta = \mu_0 + \frac{\tau_y}{\sqrt{\frac{1}{2}(\dot{\gamma}:\dot{\gamma})}}(1-\exp(-m\sqrt{\tfrac{1}{4}(\dot{\gamma}:\dot{\gamma})})) \tag{7}$$

where m is the exponential growth parameter. In particular, Abdali *et al.* [14] demonstrated that equation (7) adequately approximates an ideal Bingham plastic fluid. In fact, from the computational point of view, equation (7) is simple to implement and gives a good approximation in the limit of low shear rate. Therefore, in the present study, we are to use equation (7) with $m = 1000$.

The non-dimensionalized governing equations for axisymmetric flow in cylindrical coordinates are

$$\frac{\partial u}{\partial x} + \frac{v}{r} + \frac{\partial v}{\partial r} = 0 \tag{8}$$

$$\frac{\partial u}{\partial t}+u\frac{\partial u}{\partial x}+v\frac{\partial u}{\partial r}=-\frac{\partial p}{\partial x}+\frac{1}{Re}\left(\frac{\partial}{\partial x}\left(\eta_{\text{eff}}\cdot 2\frac{\partial u}{\partial x}\right)+\frac{1}{r}\frac{\partial}{\partial r}r\left(\eta_{\text{eff}}\cdot\left(\frac{\partial u}{\partial r}+\frac{\partial v}{\partial x}\right)\right)\right) \quad (9a)$$

$$\frac{\partial v}{\partial t}+u\frac{\partial v}{\partial x}+v\frac{\partial v}{\partial r}=-\frac{\partial p}{\partial r}+\frac{1}{Re}\left(\frac{\partial}{\partial x}\left(\eta_{\text{eff}}\cdot\left(\frac{\partial u}{\partial r}+\frac{\partial v}{\partial x}\right)\right)-\frac{1}{r}\left(\eta_{\text{eff}}\cdot 2\frac{v}{r}\right)+\frac{1}{r}\frac{\partial}{\partial r}r\left(\eta_{\text{eff}}\cdot 2\frac{\partial v}{\partial r}\right)\right) \quad (9b)$$

$$\frac{\partial\Theta}{\partial t}+u\frac{\partial\Theta}{\partial x}+v\frac{\partial\Theta}{\partial r}=\frac{2}{Pe}\left(\frac{\partial^2\Theta}{\partial x^2}+\frac{1}{r}\frac{\partial}{\partial r}\left(r\frac{\partial\Theta}{\partial r}\right)\right)+\frac{2Br}{Pe}\eta_{\text{eff}}\left(\tfrac{1}{2}(\dot\gamma^*:\dot\gamma^*)\right) \quad (10)$$

$$\eta_{\text{eff}}=1+\frac{Y}{\sqrt{\frac{1}{2}(\dot\gamma^*:\dot\gamma^*)}}\left(1-\exp\left(-m\sqrt{\tfrac{1}{2}(\dot\gamma^*:\dot\gamma^*)}\right)\right) \quad (11)$$

$$\tfrac{1}{2}(\dot\gamma^*:\dot\gamma^*)=2\left(\left(\frac{\partial u}{\partial x}\right)^2+\left(\frac{v}{r}\right)^2+\left(\frac{\partial v}{\partial r}\right)^2\right)+\left(\frac{\partial u}{\partial r}+\frac{\partial v}{\partial x}\right)^2 \quad (12)$$

where $\eta_{\text{eff}}=\eta/\mu_0$ is the non-dimensionalized apparent viscosity and $Y=\tau_y R/\mu_0 U_{\text{av}}$ is the yield number. Vradis *et al.* [7] neglected the term $-(1/r)\cdot\eta_{\text{eff}}\cdot 2(v/r)$ on the right-hand side of equation (9b) without any explanations and possibly by mistake. Furthermore, their definition of Reynolds number is somewhat unclear. Effects of neglecting the term $-(1/r)\cdot\eta_{\text{eff}}\cdot 2(v/r)$ will be discussed in Section 4.

The calculation domain and boundary conditions are shown in Fig. 1. It is assumed that the velocity and temperature are uniform at the inlet and are fully developed at the outlet. No-slip and constant temperature conditions are applied at the wall. Vradis *et al.* [7] assumed $\partial\Theta/\partial x=0$ for thermally fully developed flow condition. However, in order to satisfy this condition at the outlet, the calculation domain must be stretched unnecessarily long. Thus, we prefer to impose $\partial(\Theta/\Theta_m)/\partial x=0$ rather than $\partial\Theta/\partial x=0$ at the outlet.

For hydrodynamically developing flow problem, we consider only equations (8) and (9) subject to necessary boundary conditions, while for simultaneously developing flow problem, we consider the entire system of equations and boundary conditions.

3. NUMERICAL METHOD

The governing equations (8)–(10) are integrated in time using a fully implicit four-step fractional method [16]:

$$\frac{\hat U_i-U_i^n}{\Delta t}+\frac{1}{2}\frac{\partial}{\partial x_j}(\hat U_i\hat U_j+U_i^nU_j^n)=-\frac{1}{\rho}\frac{\partial P^n}{\partial x_i}+\frac{1}{2\rho}\frac{\partial}{\partial x_j}(\hat\tau_{ij}+\tau_{ij}^n) \quad (13)$$

$$\frac{U_i^*-\hat U_i}{\Delta t}=\frac{1}{\rho}\frac{\partial P^n}{\partial x_i} \quad (14)$$

$$\frac{\partial^2}{\partial x_j^2}P^{n+1}=\frac{\rho}{\Delta t}\frac{\partial U_i^*}{\partial x_i} \quad (15)$$

$$\frac{U_i^{n+1}-U_i^*}{\Delta t}=-\frac{1}{\rho}\frac{\partial P^{n+1}}{\partial x_i} \quad (16)$$

$$\frac{T^{n+1}-T^n}{\Delta t}+\frac{1}{2}\frac{\partial}{\partial x_j}(T^{n+1}U_j^{n+1}+T^nU_j^n)=\frac{1}{2}\alpha\frac{\partial^2}{\partial x_j^2}(T^{n+1}+T^n)+\frac{(\eta\cdot\Phi)^n}{\rho C_p} \quad (17)$$

where Δt is the time increment, $\hat U_i$ and U_i^* are intermediate velocities and superscript n denotes the time level. The convection and diffusion terms are integrated using the Crank–Nicolson method (second-order accuracy).

The fact that the pressure is decoupled from the velocity in the fractional step method was utilized successfully in the finite element analysis of the incompressible Navier–Stokes equations by several researchers [17–21]. In the fractional step method, the coefficient of the pressure equation is fixed and the inverse matrix of the pressure equation does not need to be calculated at every iteration like the SIMPLE procedure [8]. The boundary condition of $\hat U_i$ is given

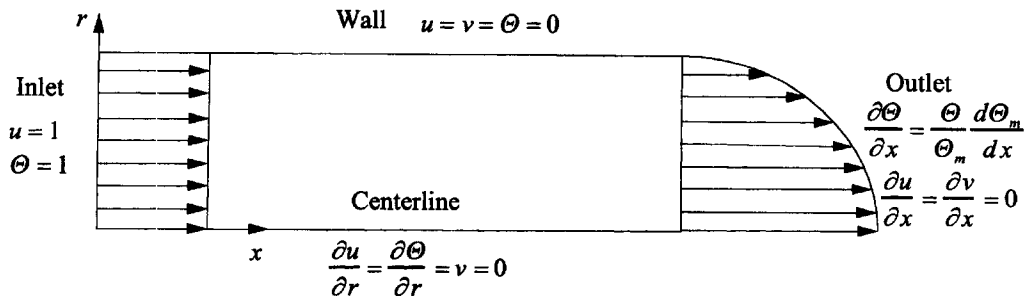

Fig. 1. Computational domain and boundary conditions.

as U_i^{n+1} within the second-order accuracy [16], as can be derived from equations (14) and (16):

$$\hat{U}_i = U_i^{n+1} + \Delta t \frac{\partial (P^{n+1} - P^n)}{\partial x_i} = U_i^{n+1} + O(\Delta t^2). \tag{18}$$

The momentum and pressure equations are discretized using a Galerkin method and the energy equation using a consistent streamline upwind Petrov–Galerkin method [22]. In obtaining the linear algebraic equation from the nonlinear momentum equations, the successive approximation method [23] is used. The discretized momentum and energy equations are solved by using a line-by-line TDMA, with the pressure equation solved by using a line SOR (successive over-relaxation).

From the continuity constraint, we obtain a Poisson type pressure equation. Since we use an equal order velocity pressure formulation, the weighting function of the continuity equation must be of the same order as that of the momentum equation. Then, applying the method of weighted residuals, the continuity equation is expressed as follows:

$$\int_{A_e} w \nabla \cdot \mathbf{U}^{n+1} \, dA_e = 0. \tag{19}$$

By the vector identity $(\nabla \cdot (\mathbf{U}w) = \nabla w \cdot \mathbf{U}^{n+1} + w \nabla \cdot \mathbf{U}^{n+1})$ and the divergence theorem, equation (19) is rewritten as follows:

$$\int_{A_e} \nabla w \cdot \mathbf{U}^{n+1} \, dA_e = \int_{S_e} (w \mathbf{U}^{n+1} \cdot \mathbf{n}) \, dS_e. \tag{20}$$

Then, substituting equation (16) into equation (20), the following Poisson type pressure equation is obtained.

$$\frac{\Delta t}{\rho} \int_{A_e} \left(\frac{\partial w}{\partial x_j} \frac{\partial P^{n+1}}{\partial x_j} \right) dA_e = \int_{A_e} \left(\frac{\partial w}{\partial x_j} U_j^* \right) dA_e - \int_{S_e} (w \mathbf{U}^{n+1} \cdot \mathbf{n}) \, dS_e. \tag{21}$$

A typical weak formulation of the pressure equation used by other investigators [18, 21] is written by considering equation (15):

$$\int_{A_e} \left(\frac{\partial w}{\partial x_j} \frac{\partial P^{n+1}}{\partial x_j} \right) dA_e = -\frac{\rho}{\Delta t} \int_{A_e} \left(\frac{\partial U_j^*}{\partial x_j} w \right) dA_e + \int_{S_e} w \frac{\partial P^{n+1}}{\partial n} dS_e. \tag{22}$$

From numerical experiment, we note that equation (21) is preferable to equation (22) in treating outlet boundary conditions.

4. RESULTS AND DISCUSSION

For hydrodynamically developing flow problem, an 81×21 non-uniform mesh is used, where the axial length is 8 times the pipe radius. For the simultaneously developing flow problem, a 121×21 non-uniform mesh is used, where the axial length is 50 times the pipe radius. The steady state solution is obtained when the following condition is satisfied

$$e_{max} = \max_{i=1,N_t} |\varphi_i^n - \varphi_i^{n-1}| < 10^{-9} \tag{23}$$

where φ denotes the normalized variables, the subscript i denotes the specific node point, the superscript n denotes the time level and N_t denotes the total number of nodes.

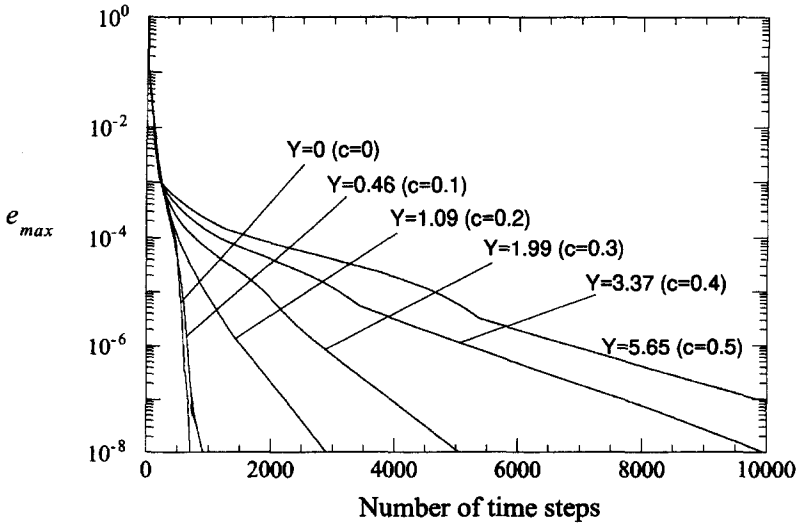

Fig. 2. Convergence history for various yield numbers.

4.1. *Hydrodynamically developing flow*

Figure 2 shows the convergence histories for $Y = 0$, 0.46, 1.09, 1.99, 3.37 and 5.65 and for $Re = 25$. It shows that more time steps are required to reach the steady state for larger Y. Figure 3 shows the velocity profiles at the outlet of a pipe, where hydrodynamically fully developed flow is assumed. It is noted that good agreements are achieved between the previous analytical [9] and the present numerical solutions. Also note that there is a uniform velocity region near the centerline, namely 'plug flow' or 'core' region, when Y is non-zero. The plug flow region becomes wider with the increase of Y. The yield number Y can be written in terms of the core radius c as follows [5]:

$$Y = \frac{12c}{3-4c+c^4}. \tag{24}$$

The radial variations of the axial velocity at four axial locations are shown in Fig. 4. Near the inlet, the velocity profile has a local minimum at the pipe centerline and a local maximum near the wall. Such velocity overshoots were first reported for Newtonian fluids by Wang and Longwell [24] and further explained in Shah and London [1]. Note that the velocity overshoot is attenuated by the increase of Y.

Figure 5 shows the variation of the axial velocity along the centerline, together with other researchers' results. In the numerical analysis, the velocity profile must linearly fall from a constant value to zero within the nearest element to the wall at the inlet to satisfy the no-slip condition. This causes the centerline velocity at the inlet to be slightly larger than the inlet bulk velocity. It is shown that, as the yield number increases, the velocity develops faster, resulting in shorter entrance length. When $Y = 0$ (laminar Newtonian fluid flow), the present result shows good agreement with that of Benim and Zinser [25]. Also, it is revealed that the boundary layer approximation used in Chen *et al.* [5] is not accurate in predicting the flow in the inlet region. Note that the results of Vradis *et al.* [7] are very different from those of the present study and Benim and Zinser [25], which is believed to be the consequence of neglecting a term in the governing equations (see also Sections 1 and 2).

The contours of effective viscosity for different values of Y are shown in Fig. 6, where the dotted lines indicate the unyielded regions, or plug flow regions. It is interesting to note that for large values of Y, the apparent viscosity along the centerline rapidly increases near $x = 1$, while the apparent viscosity along the wall increases monotonically and relatively slowly. From equations (11) and (12), it is noted that the viscosity along the centerline is affected only by $\partial u/\partial x$ because $\partial u/\partial r = v = \partial v/\partial x = 0$ there. An abrupt increase of the apparent viscosity along the centerline is due to the fact that the velocity becomes fully developed near $x = 1$, so that $\partial u/\partial x \approx 0$, making the denominator of the second term on the right-hand side of the equation (and hence, that of equation (11)) become zero.

Figure 7 shows isobars for different values of Y. It is noteworthy that adverse pressure gradients appear near $x = 1$, when $Y > 4$. This phenomenon is explained as follows: along the centerline, the x-momentum equation (9a) becomes,

$$\frac{\partial p}{\partial x} = \frac{2}{Re}\left(\frac{\partial \eta_{\text{eff}}}{\partial x}\frac{\partial u}{\partial x} + \eta_{\text{eff}}\frac{\partial^2 u}{\partial x^2}\right) - u\frac{\partial u}{\partial x} \tag{25}$$

where $\partial \eta_{\text{eff}}/\partial x$ is very large near $x = 1$ for large values of Y (Fig. 6) so that $\partial p/\partial x > 0$. However, the yielded regions naturally coincide with favorable pressure gradient regions and the occurrence of an adverse pressure gradient can be considered as an indication of the start of the plug flow region.

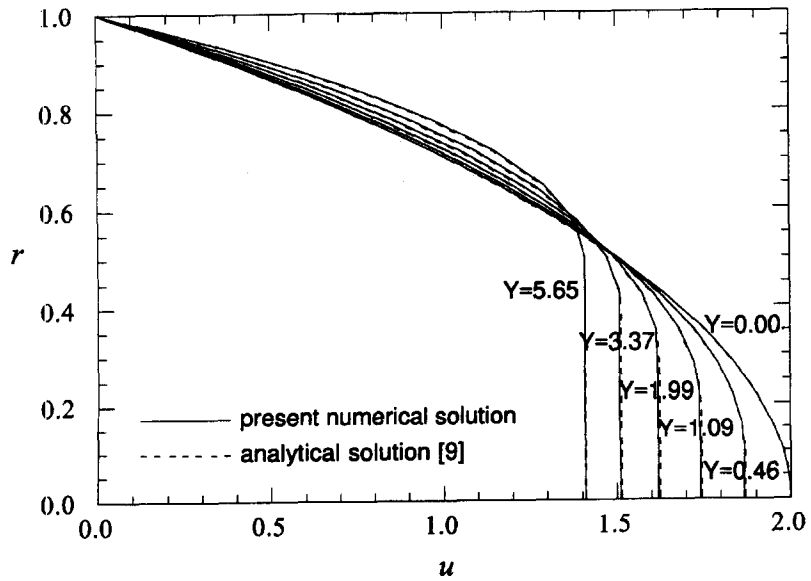

Fig. 3. Fully developed velocity profiles.

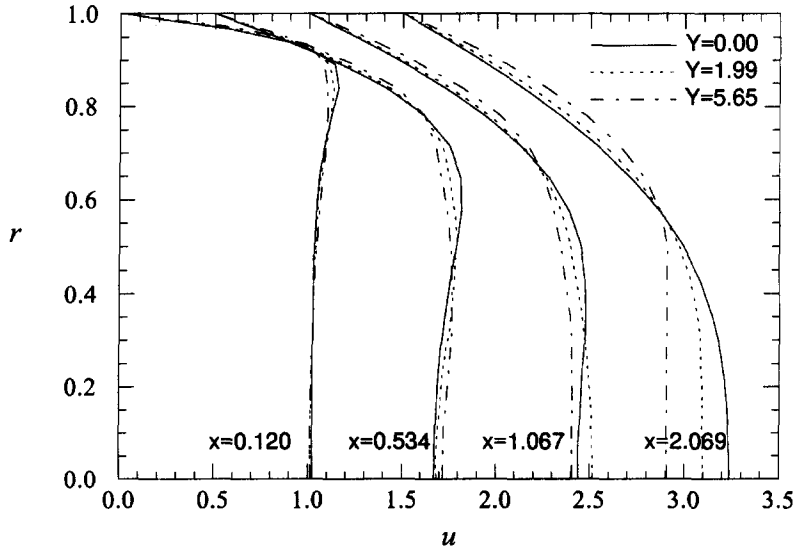

Fig. 4. Radial variations of the axial velocity at four axial locations.

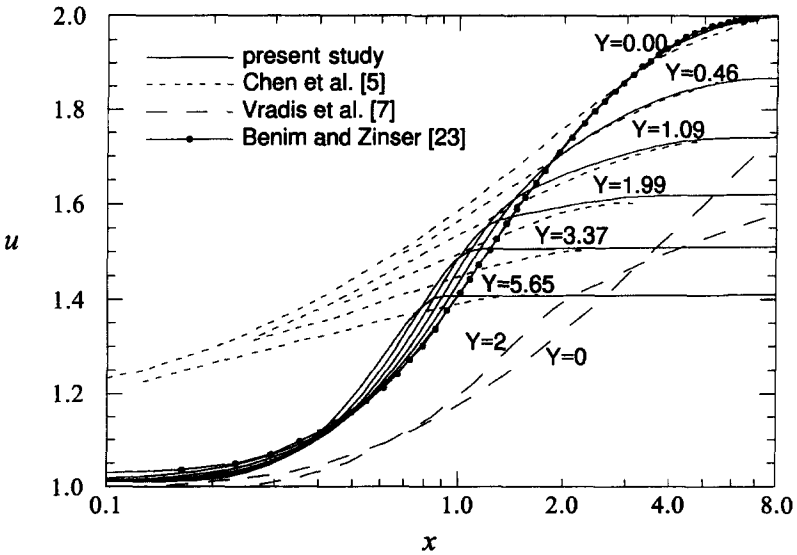

Fig. 5. Variations of centerline velocity with respect to axial distance.

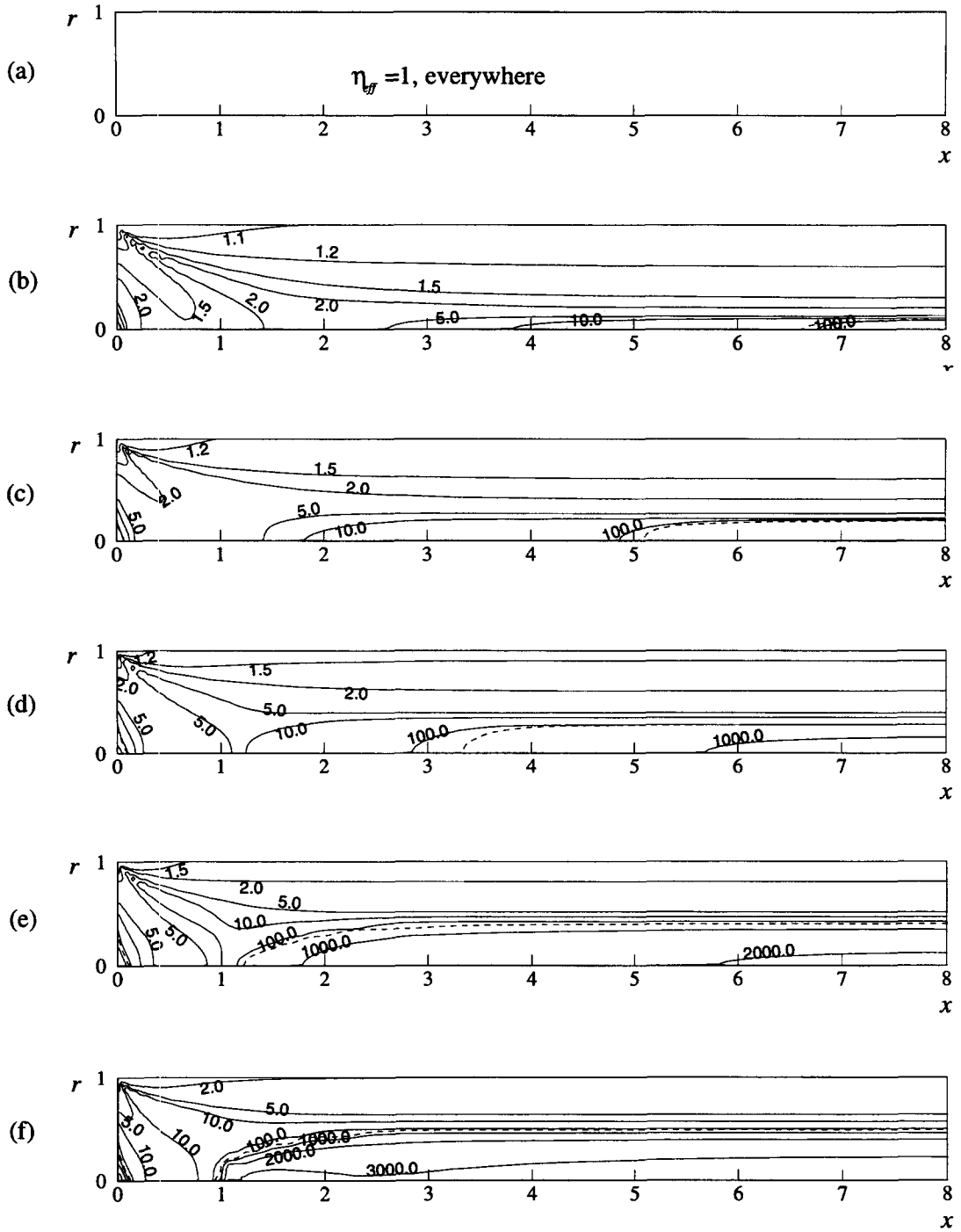

Fig. 6. Contours of effective viscosity for different values of Y, where the dotted lines indicate the unyielded regions around the centerline: (a) $Y = 0$; (b) $Y = 0.46$; (c) $Y = 1.09$; (d) $Y = 1.99$; (e) $Y = 3.37$; (f) $Y = 5.65$.

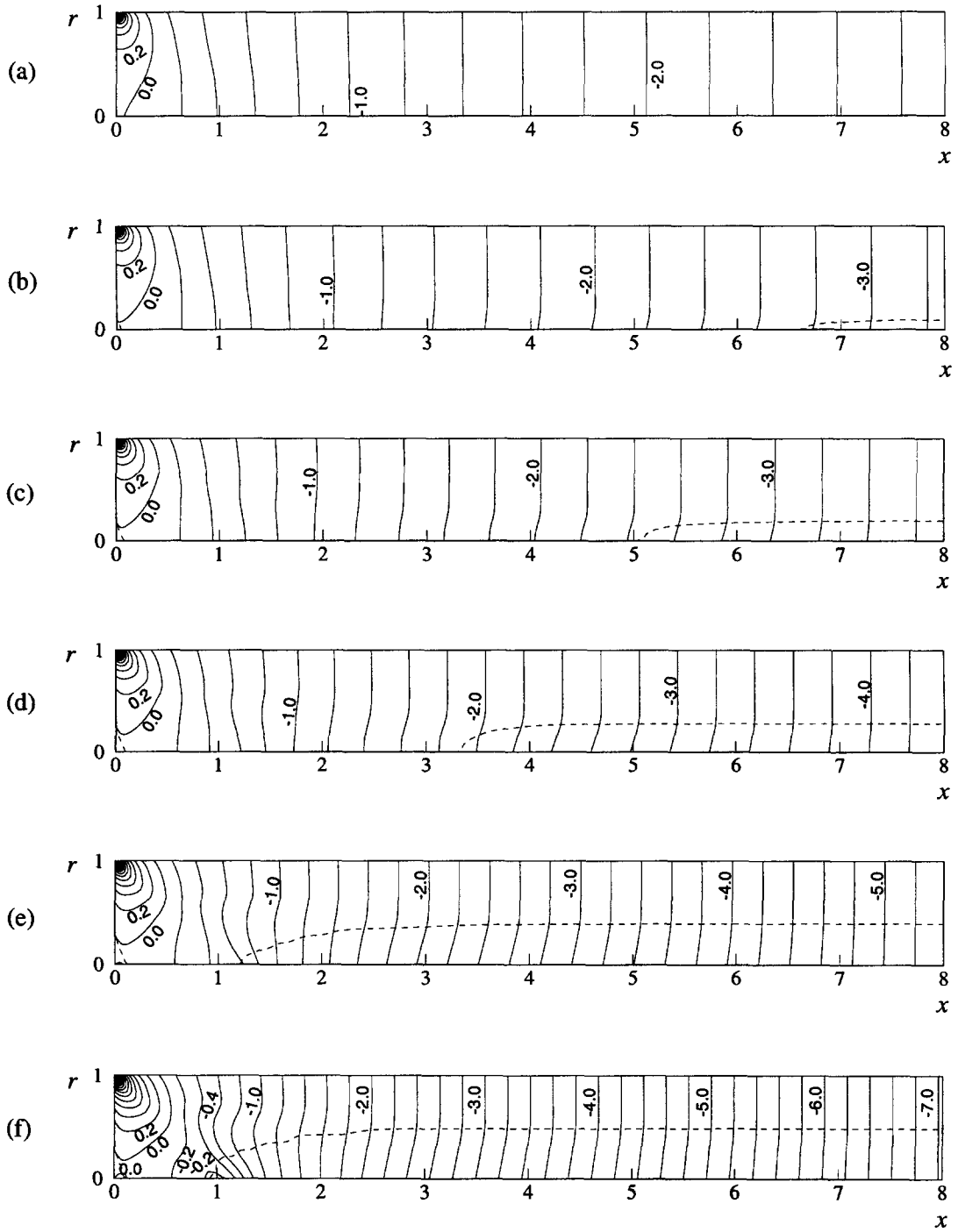

Fig. 7. Isobars for different values of Y, where the dotted lines indicate the unyielded regions around the centerline: (a) $Y = 0$; (b) $Y = 0.46$; (c) $Y = 1.09$; (d) $Y = 1.99$; (e) $Y = 3.37$; (f) $Y = 5.65$.

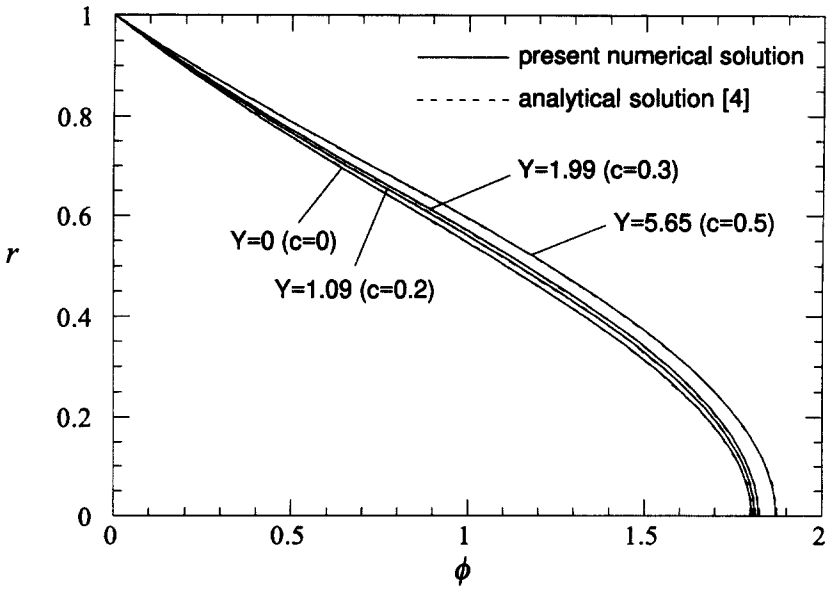

Fig. 8. Fully developed temperature profiles.

4.2. *Simultaneously developing flow*

Figure 8 shows the temperature profiles at the outlet of the computational domain where simultaneously (hydrodynamically and thermally) fully developed flow is assumed. The numerical solutions of the present study agree well with the fully developed temperature profiles obtained from an analytical study [4]. It shows both the validity of the present numerical method and that of the thermally fully developed flow assumption.

Figure 9 shows the local Nusselt number Nu for $Y = 1.99$ and $Re = 5, 25, 50$. In the present study, the local Nusselt number Nu is defined as

$$Nu = -\frac{2}{\Theta_m}\frac{\partial\Theta}{\partial r}\bigg|_{r=1} \tag{26}$$

Theoretically, the local Nusselt number at the inlet of a pipe is infinite because the temperature gradient at the wall is infinite. For the same Prandtl number, the velocity and temperature fields develop faster for lower Re. Hence, higher Nu is expected for higher Re in the entrance region. In Fig. 9(a), the local Nusselt number is shown to be higher for higher Re. However, these results seem to be different from those of the previous study [4] which predicted higher Nu for lower Pe ($=2\ Re\ Pr$). Note that the axial coordinate in Fig. 9(a) is not x^+, but x. If the curves in Fig. 9(a) are represented with the Graetz type axial coordinate x^+, those curves show the same trend as those predicted in the previous study [4] (Fig. 9(b)).

Figure 10 shows the local Nusselt number for $Y = 1.99$ and $Pr = 1, 2, 5, 10$ together with an analytical solution obtained for $Pe \to \infty$ [26]. In the case of Newtonian fluid flow, it is known that for a Prandtl number larger than 5, the fully developed velocity assumption (the Graetz problem idealization) introduces little error because the velocity profile develops so much faster than the temperature profile [3]. Figure 10 also shows that one can assume that the velocity field is fully developed when $Pr > 10$ for a Bingham plastic. Note that there exists a substantial difference between the present result and the result from Vradis *et al.* [7].

Figure 11 shows the local Nusselt number along the axial distance for $Y = 0$, 1.99, 5.65 when $Re = 25$, $Pr = 1$ and $Br = 0$. As is in the previous study [4], the Nusselt number of a Bingham plastic is not significantly affected by the yield stress when viscous dissipation is excluded.

Figures 12(a) and (b) shows the bulk temperature and local Nusselt number with respect to axial distance, respectively. The numerical results show the same trend as the analytical results of Ref. [4] where the velocity is assumed to be fully developed. In particular, it is noted that unlike the case for $Br = 0$, the Nusselt number is significantly changed by the yield stress with the inclusion of viscous dissipation.

5. CONCLUSION

Hydrodynamically developing and simultaneously developing flow problems for a Bingham plastic in laminar pipe flow are investigated by a numerical method, which uses a four-step fractional method combined with an equal order bilinear finite element method. For numerical stability reasons, a recently proposed viscosity model by Papanastasiou [15] is adopted because the viscosity function of the classical Bingham plastic model is discontinuous at the low shear rate region.

Results for various values of the yield stress, the Prandtl, Reynolds and Brinkman numbers are illustrated. The validity of the present numerical method has been verified by comparing the data for some

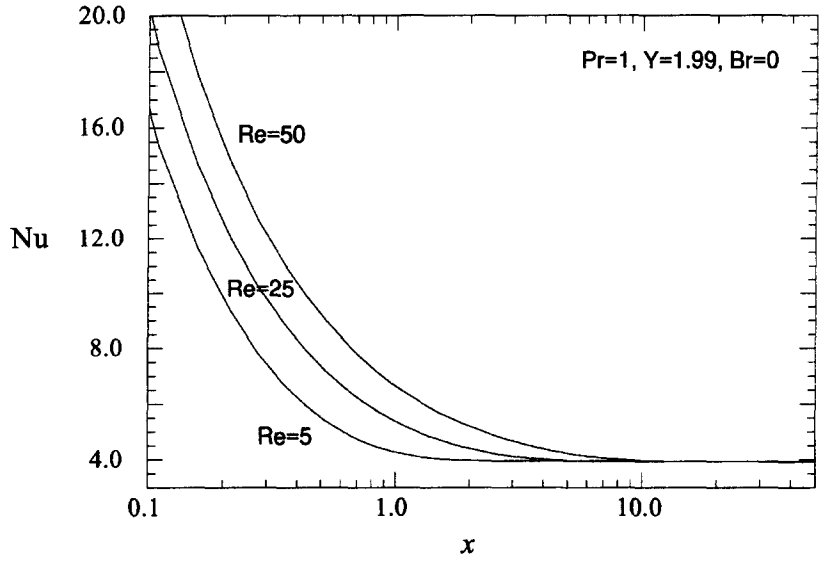

(a)

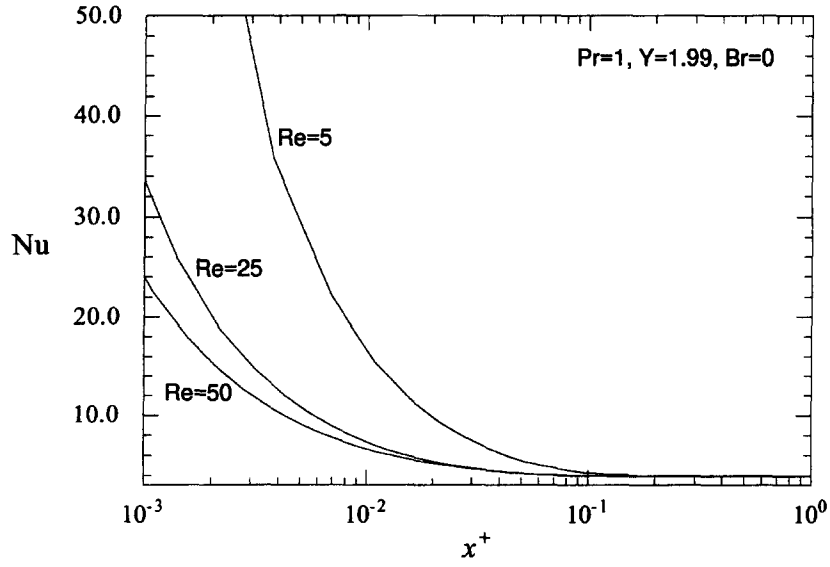

(b)

Fig. 9. Local Nusselt number: (a) with respect to dimensionless axial distance x; (b) with respect to dimensionless axial distance x^+.

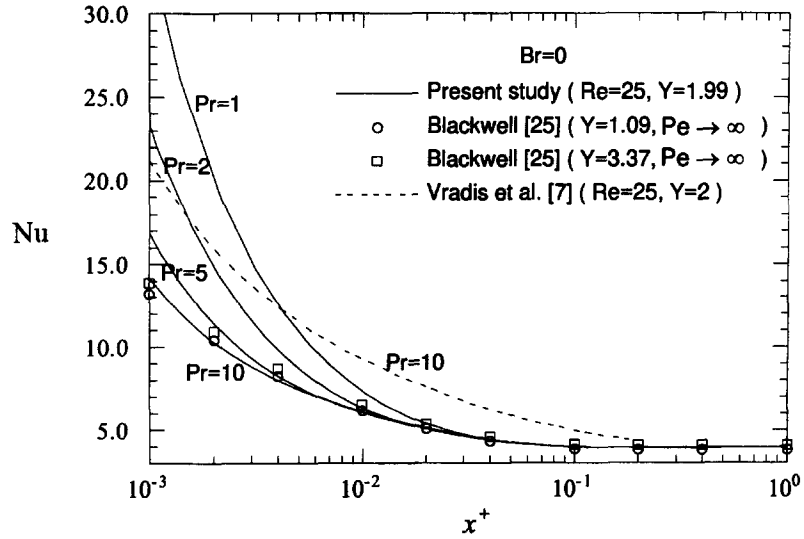

Fig. 10. Local Nusselt number with respect to axial distance for various values of Pr.

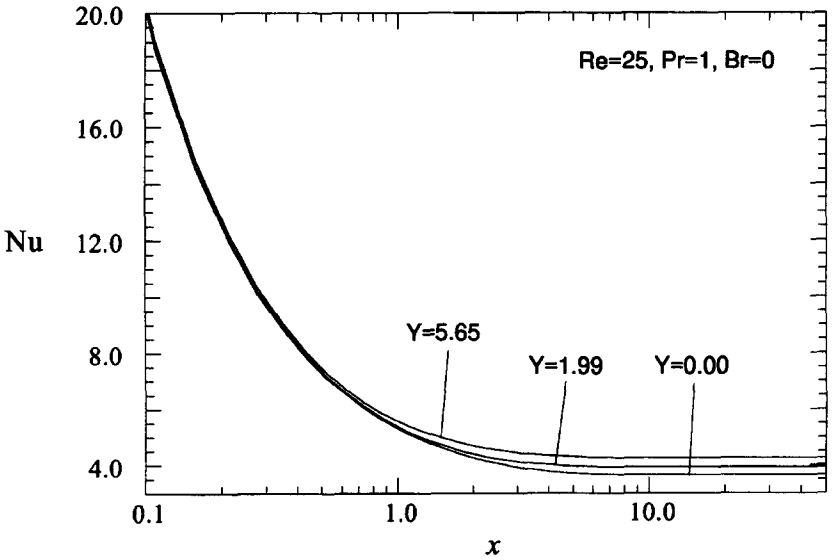

Fig. 11. Local Nusselt number with respect to axial distance for various values of Y.

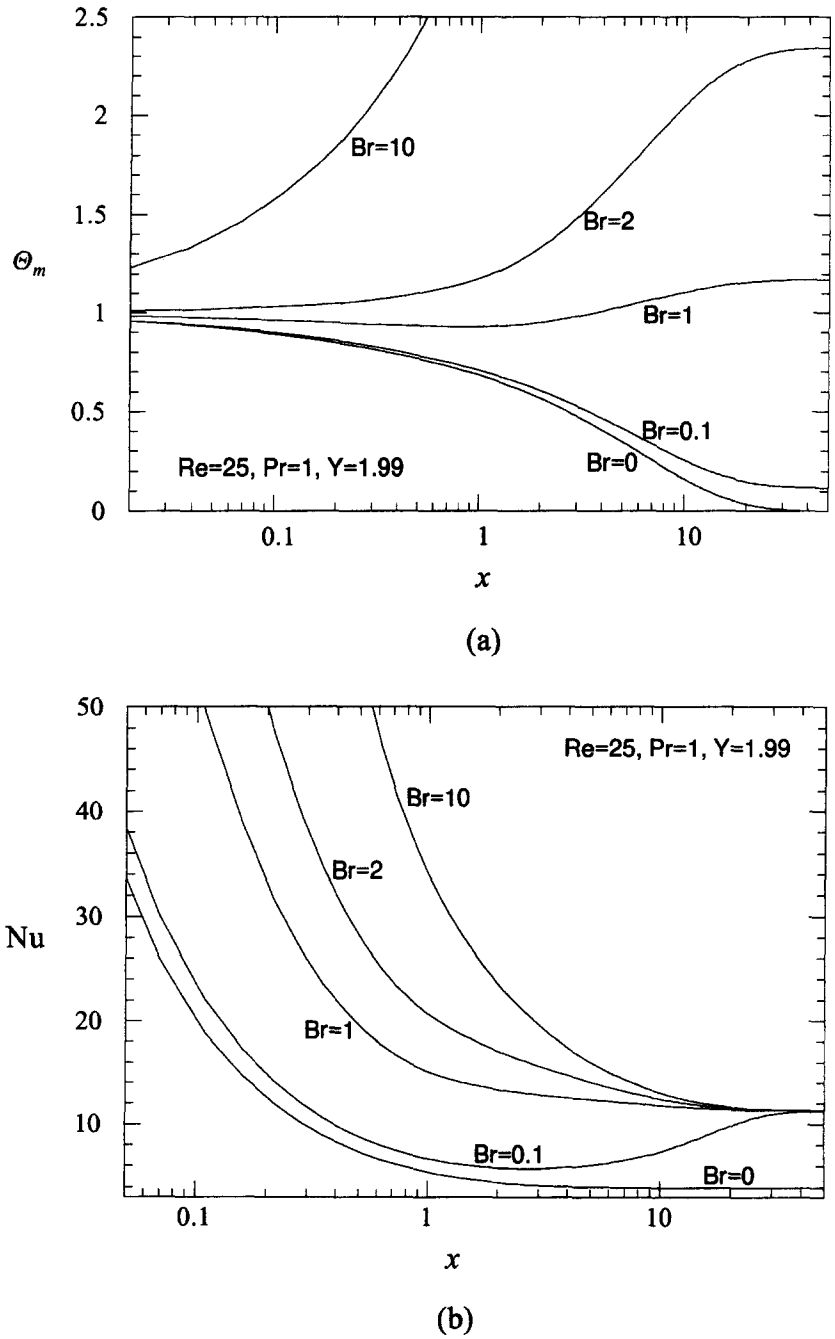

Fig. 12. (a) Bulk temperature with respect to axial distance; (b) local Nusselt number with respect to axial distance.

selected cases, wherever previous results are available. For hydrodynamically developing flow, it is shown that shorter entrance length is required to reach fully developed velocity field for larger yield stress. The unyielded region around the centerline becomes thicker and approaches the inlet as the yield stress becomes larger. For simultaneously developing flow, the heat transfer characteristics show the same trends as those predicted from the analytical method for the Graetz problem.

Acknowledgement—This study has been supported by the Department of Education, Republic of Korea.

REFERENCES

1. Shah, R. K. and London, A. L., Laminar flow forced convection in ducts. *Advances in Heat Transfer* (suppl. 1). Academic Press, New York, 1978.
2. Kakac, S., Shah, R. K. and Aung, W., *Handbook of Single-Phase Convective Heat Transfer*. Wiley, New York, 1987.

3. Kays, W. M. and Crawford, M. E., *Convective Heat and Mass Transfer*, 3rd edn. McGraw-Hill, New York, 1993.
4. Min, T., Yoo, J. Y. and Choi, H., Laminar convective heat transfer of a Bingham plastic in a circular pipe—I. Analytical approach—thermally fully developed flow and thermally developing flow (the Graetz problem extended). *International Journal of Heat and Mass Transfer* 1997, **40,** 3025–3037.
5. Chen, S. S., Fan, L. T. and Hwang, C. L., Entrance region flow of the Bingham fluid in a circular pipe. *AIChE Journal*, 1970, **16,** 293–299.
6. McDonald, J. W., Denny, V. E. and Mills, A. F., Numerical solutions of the Navier–Stokes equations. *Journal of Applied Mechanics*, 1972, **94,** 873–878.
7. Vradis, G. C., Dougher, J. and Kumar, S., Entrance pipe flow and heat transfer for a Bingham plastic. *International Journal of Heat and Mass Transfer*, 1993, **36,** 543–552.
8. Choi, H. G., Choi, H. and Yoo, J. Y., A fractional four-step finite element formulation of the unsteady incompressible Navier–Stokes equations using SUPG and linear equal order element methods, *Computer Methods in Applied Mechanics and Engineering*, (in press).
9. Bird, R. B., Stewart, W. E. and Lightfoot, E. N., *Transport Phenomena*. Wiley, New York, 1960.
10. Bird, R. B., Curtiss, C. F., Armstrong, R. C. and Hassager, O., *Dynamics of Polymeric Liquids*. Wiley, New York, 1987.
11. Darby, R., *Viscoelastic Fluid*. Dekker, New York, 1976.
12. Beverly, C. R. and Tanner, R. I., Numerical analysis of three-dimensional Bingham plastic flow. *Journal of Non-Newtonian Fluid Mechanics*, 1992, **42,** 85–115.
13. Ellwood, K. R. J., Georgiou, G. C., Papanastasiou, T. C. and Wilkes, J. O., Laminar jets of Bingham-plastic liquids. *Journal of Rheology*, 1990, **34,** 787–812.
14. Abdali, S. S., Mitsoulis, E. and Markatos, N. C., Entry and exit flows of Bingham fluids. *Journal of Rheology*, 1992, **36,** 2, 389–407.
15. Papanastasiou, T. C., Flows of materials with yield. *Journal of Rheology*, 1987, **31,** 385–404.
16. Choi, H. and Moin, P., Effects of the computational time step on numerical solutions of turbulent flow. *Journal of Computational Physics*, 1994, **113,** 1–4.
17. Donea, J., Giuliani, S., Laval, H. and Quartapelle, L., Fine element solution of the unsteady Navier–Stokes equation by a fractional step method. *Computer Methods in Applied Mechanics and Engineering*, 1982, **30,** 53–73.
18. Ramaswamy, B., Finite element solution for advection and natural convection flow. *Computers and Fluids*, 1988, **16,** 349–388.
19. Ramaswamy, B. and Jue, T. C., Some recent trends and developments in finite element analysis for incompressible thermal flow. *International Journal of Numerical Methods in Engineering*, 1992, **35,** 671–707.
20. Kawahara, M. and Ohmiya, K., Finite element analysis of density flow using the velocity correction method. *International Journal for Numerical Methods in Fluids*, 1985, **5,** 981–993.
21. Zienkiewicz, O. C. and Wu, J., Incompressibility without tears—how to avoid restrictions of mixed formulation. *International Journal of Numerical Methods in Engineering*, 1991, **32,** 1189–1203.
22. Brooks, A. N. and Hughes, T. J. R., Streamline upwind Petrov-Galerkin formulation for convection dominated flows with particular emphasis on the incompressible Navier–Stokes equations. *Computer Methods in Applied Mechanics and Engineering*, 1982, **32,** 199–259.
23. Carey, G. F. and Oden, J. T., *Finite Elements: Fluid Mechanics*, Vol. 6. Prentice-Hall, New Jersey, 1986, pp. 168–170.
24. Wang, Y. L. and Longwell, P. A., Laminar flow in the inlet section of parallel plates. *AIChE Journal*, 1964, **10,** 323–329.
25. Benim, A. C. and Zinser, W., A segregated formulation of Navier–Stokes equations with finite elements. *Computer Methods in Applied Mechanics and Engineering*, 1986, **57,** 223–237.
26. Blackwell, B. F., Numerical solution of the Graetz problem for a Bingham plastic in laminar tube flow with constant wall temperature. *Journal of Heat Transfer*, 1985, **107,** 466–468.